이학석사학위논문

Time Resolved Spectroscopic Study of Photocurrent Generation of Phospholipid Assembled DSSN+

인지질에 집적된 DSSN+의
광전류 생성에 대한 시분해 분광학 연구

2013년 2월

서울대학교 대학원

화학부 물리화학전공

이 정 은

Time Resolved Spectroscopic Study of Photocurrent Generation of Phospholipid Assembled DSSN+

지도교수 김 성 근

이 논문을 이학석사 학위논문으로 제출함

2013년 2월

서울대학교 대학원
화학부
이 정 은

이정은의 이학석사 학위논문을 인준함

2013년 2월

위 원 장 서 정 쌍 (인)
부위원장 김 성 근 (인)
위 원 신 석 민 (인)

ABSTRACT

Time Resolved Spectroscopic Study of Photocurrent Generation of Phospholipid Assembled DSSN+

Jung Eun Lee

Department of Chemistry

The Graduate School

Seoul National University

Time-resolved spectroscopic study has attracted a significant amount of interest in the past several decades because it provides the essential information to fully understand photophysical properties of compounds in the excited state. We introduced time-resolved spectroscopic techniques such as femtosecond transient absorption and time-correlated single photon counting spectroscopy to study dynamics and the lifetime occurring in the excited state. To demonstrate the feasibility of these techniques, we applied to study about energy transfer in molecular photovoltaic devices.

In this study, we implemented water-based artificial photovoltaic system using conjugated oligoelectrolytes and a dye. We used 4,4'-bis(4'-(N,N-bis(6''-(N,N,N-trimethylammonium)hexyl) amino)-styryl)stilbene tetraiodide (DSSN+) as a donor and Nile red as an acceptor. DSSN+ and Nile red are intercalated into DMPC vesicle and we investigated the energy transfer from DSSN+ to Nile red using steady-state

photoluminescence, time-correlated single photon counting and transient absorption techniques. In this vesicle system, the value of fluorescence resonance energy transfer (FRET) efficiency between the donor and the acceptor is considerable. Moreover, we studied the photocurrent generation in an optimized photovoltaic system.

Keywords: Transient Absorption Spectroscopy, Time-Correlated Single Photon Counting, Fluorescence Resonance Energy Transfer, DSSN+, Photocurrent

Student Number : 2011-20301

Table of Contents

국문초록

Acknowledgements (감사의 글)

1. Introduction

In physics and physical chemistry, time-resolved spectroscopy has been a fascinating study of dynamic processes in chemical compounds or materials such as fluorophores and quantum dots using spectroscopic techniques. Time-resolved spectroscopy provides important information on lifetime, indirect mechanism of energy transfer and the excited state dynamics of materials or chemical compounds. These information is very essential in many fields such as solar cell study because they are intensively related to energy efficiency. With the help of pulsed lasers, we can study processes that occur on time scales as short as 10^{-16} seconds. Most of the excited state dynamics happens in the range from less than 100 fs to 100 ps. Depending on the time scale, various time-resolved spectroscopic techniques is applied. One of the most popular techniques is transient absorption (TA) spectroscopy which is a pump-probe technique. Pump pulse is for excitation of molecules in the ground state and probe pulse is for measuring the absorbance changes. Using TA technique, we can obtain the information on the dynamics of both emissive and non-emissive states compare to time-resolved fluorescence techniques.

In this study, we employed TA spectroscopy to investigate the energy transfer dynamics in DMPC vesicle system that both a donor and an acceptor molecules are embedded. Moreover, to support TA results, time-correlated single photon counting (TCSPC) techniques was used. In here, the fluorescence lifetime was an indicator of the energy transfer from the donor to the acceptor.

2. Basic Principles

2.1 Transient Absorption Spectroscopy

Transient absorption (TA) spectroscopy is a pump-probe technique and sensitive technique to study of dynamics occurring in the excited states and the lifetime of short living species. In a pump-probe transient absorption experiment, pump pulse and probe pulse are incident into a sample in which they spatially overlap. The wavelength of pump pulse should overlap with the absorption range of the sample. The intense pump pulse excites the a fraction of the molecules in the ground state to the excited state, and then the weak probe pulse is passed through the sample with a delay time with respect to the pulse time. Here, the induced optical changes are monitored as a function of time by the absorption measurement of probe pulse. The signals detected by changing the time delay between the pump and the probe are used to calculate for ΔOD.

$$\Delta OD = OD\ (pump\ on) - OD\ (pump\ off)$$

A full time profile provides the information on the dynamical process such as energy transfer, charge/proton transfer, intersystem crossing and isomerization.[1,2] Compared to time-resolved fluorescence spectroscopic techniques including time-correlated single photon counting (TCSPC), TA can be used in any system. Time-resolved fluorescence spectroscopic technique can measure only with fluorescent samples, while TA can be also attainable an investigation of non-emissive states and dark states. In general, a transient absorption spectrum contains contributions from diverse processes. The first information is provided by excited-state absorption. When the wavelength of the probe pulse overlaps with the absorption range of the excited state, the probe pulse will

contribute to the optically allowed promotion from the excited state to higher excited state upon excitation with the pump pulse. The second possible information is the absorption of a transient or a long-lived state such as triplet states, charge-separated states, and isomerized state, occurred after excitation by the pump beam. Consequently, these two process will appear as a positive signal in the transient absorption spectrum. On the other hand, there are two possible processes that result in a negative signal in the time profile of the transient absorption. First would be a ground state bleach process. The number of the molecules in the ground state after excitation by the pump pulse would be decreased compared to before excitation. As a result, the ground state absorption in the excited sample is less than that in the non-excited sample, and the negative signal is observed in the wavelength region of ground state absorption. Second is the stimulated emission process. When the wavelength of the probe pulse corresponds to the energy difference between the ground state and the excited state, photon from probe pulse will induce stimulated emission to the ground state. Furthermore, it could be theoretically occurred once the Einstein coefficient for the absorption from the ground state to the excited state and the stimulated emission from the excited state to the ground state are equal.[2] By the way, the intensity of the probe pulse is so weak that stimulated emission doesn't significantly affect the results. Therefore, TA is the effective technique to study of dynamics and the lifetime in the excited state, and we should consider various process when analyzing the data.

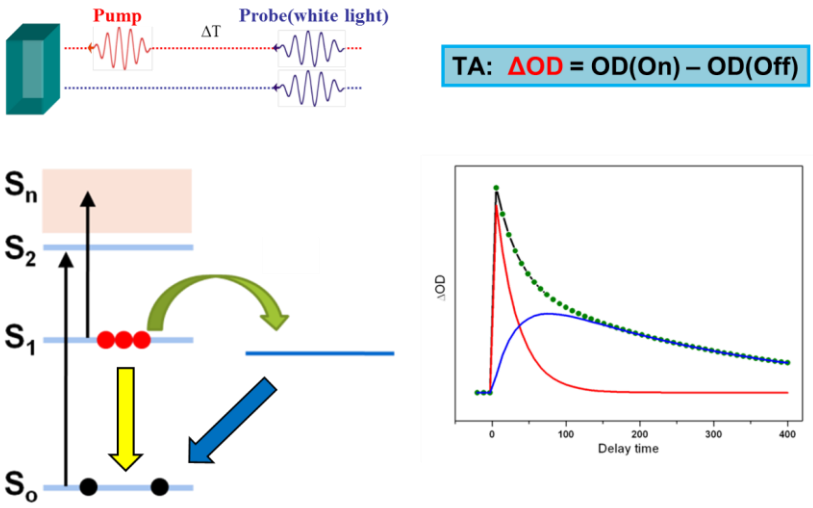

Figure 1. The concept of transient absorption spectroscopy.

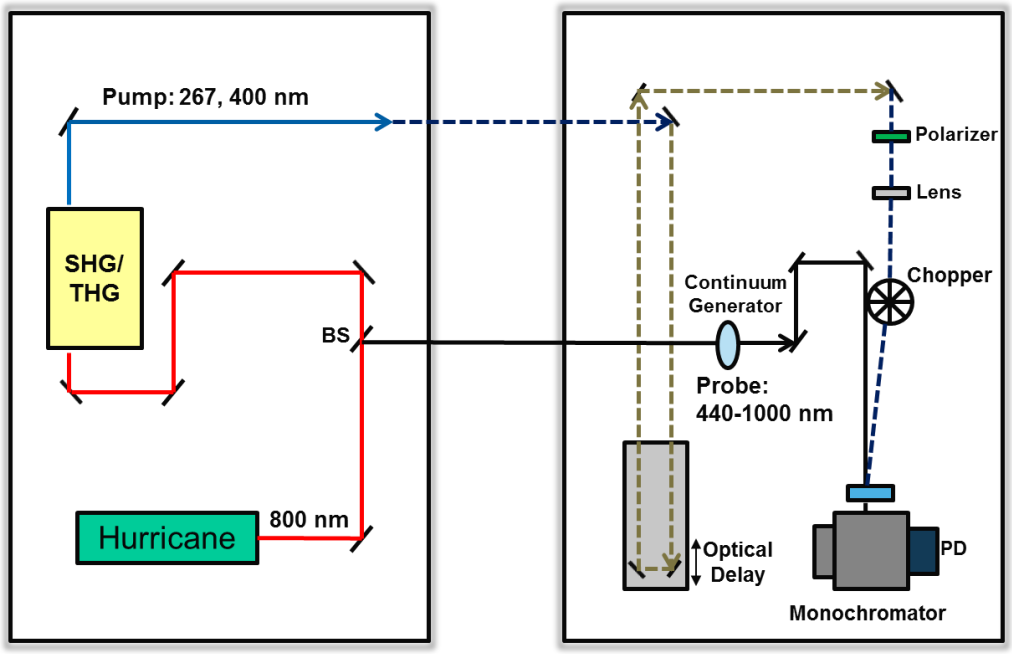

Figure 2. An experimental setup for transient absorption spectroscopy.

2.2 Time-Correlated Single Photon Counting Spectroscopy

Time-correlated single photon counting (TCSPC) is one of the best techniques of measuring the fluorescence lifetime. The principle of TCSPC is based on the detection of single photons of a periodical light signal, the measurement of detection times of the individual photons, and the reconstruction of the waveform from the individual time measurements. The sample is excited by a pulse of laser and the first photon emitted is detected by a photomultiplier tube (PMT) or avalanche photodiode (APD). One signal period contains one photon pulse. When a photon is detected, the time of the corresponding detector pulse is measured. That is, the condition of TCSPC is adapted to detect less than one photon per laser pulse. The arrival time of the observed photon is recorded as one event. After many photons, the distribution of the photons over a range of the arrival time can be plotted. The x-axis is the time difference and the y-axis is the number of photons detected for this time difference.[3] When the lifetimes of the sample are in the nanosecond range, the electronics are not fast enough to detect multiple photons. As a result of, much less than one photon is detected per excitation pulse. TCSPC has a limit to observe the short scale of lifetime. Therefore, when the lifetime is in the picosecond range, fluorescence upconversion spectroscopy, which is other techniques of measuring fluorescence lifetime, should be applied.

3. Photocurrent Generation by Fluorescence Resonance Energy Transfer between DSSN+ and Nile Red

3.1 Introduction

Lipid-assembled light-harvesting complexes on electrodes have been widely used to mimic the photosynthetic system. Many biophotonic systems such as photosystem I[4-11] or II[12-19] within the membrane of green plant, and rhodopsin proteins[20-23] embedded in the membrane of halobacteria consist of chromophores.[24-25] When light is irradiated after the immobilization of lipid-assembled light-harvesting complexes on electrode surfaces such as gold[15,16,19,26] or titanium oxide,[18,27] photocurrent can be generated by energy transfer from the complex to the electrodes. Distance or direction of complex and electrode can affect photocurrent value. The biosystems is therefore applied to photosensors,[28] phototransistors,[29] biosensors,[30] and aqueous-based photovoltaic cells.[31] Also, photocurrent generation systems based on synthetic chromophores have attracted a significant amount of interest. For instant, ruthenium bipyridine and porphyrin derivatives, popular light sensitizers, have been assembled on electrodes within phospholipid bilayers, producing a photocurrent upon photoexcitation.[32] When acceptors such as fullerene were directionally assembled on the electrodes in aqueous media by forming lipid bilayers, the photocurrent could be enhanced.[33-35]

Conjugated oligoelectrolytes (COEs) have backbones with π-delocalized electronic structures and ionic functionalities. As a result of their unique molecular structures, COEs can combine hydrophobic conjugated backbones with hydrophilic moieties and it can be

dissolved in highly polar solvents such as water or alcohols. Hydrophobic attraction could induce self-assemblies in an aqueous medium.[36] COEs have also two-photon emission characteristic, so that it is possible to be applicable to effective fluorescence imaging of living organisms.[37]

We employed the amphiphilic phenylenevinylene oligoelectrolyte 4,4'-bis(4'-(N,N-bis(6''-(N,N,N-trimethylammonium)hexyl)amino)-styryl)stilbene tetraiodide (DSSN+) as molecular wire to increase electron transport across lipid bilayers. Its structure is shown in Scheme 1. This compound is assembled with a zwitterionic phospholipid 1,2-dimyristoyl-*sn*-glycero-3-phosphocholine (DMPC).[37] The phospholipid-assembled DSSN+ significantly facilitates transmembrane electron transfer by a charge tunneling mechanism through the π-delocalized structure.

We suggested a new type of photovoltaic systems in which DSSN+ assembled in lipid bilayers as a donor and Nile red incorporated in an alkane thiol layer as an acceptor are directionally aligned on a gold electrode. Absorption spectrum of Nile red overlaps well with the emission spectrum of DSSN+ in a lipophilic environment, so that fluorescence resonance energy transfer (FRET) can occur well. As a result, photocurrent can be enhanced by FRET. In this study, we first characterized the FRET between DSSN+ and Nile red assembled in unilamellar lipid vesicles in solution. After that, we investigated the energy transfer dynamics from DSSN+ to Nile red following the photoexcitation at various intercalation ratios between the donor and acceptor using transient absorption spectroscopic technique. We also studied the photocurrent generation in an optimized photovoltaic system.

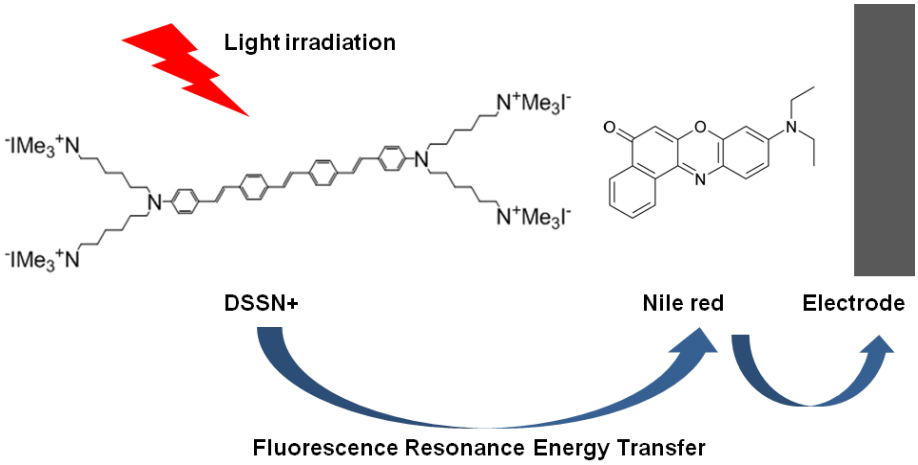

Scheme 1. Structures of DSSN+ and Nile red for fluorescence resonance energy transfer.

3.2 Experimental

1. Sample Preparation / UV-Vis, Fluorescence and Time-resolved Spectroscopy.

20 mM DMPC (Avanti Polar Lipids Inc.), 0.4 mM DSSN+ and 0.1-0.5 mM of Nile red were separately dissolved in 1 mL methanol, and then they mixed. The solvent of the mixture was completely removed by nitrogen blowing and vacuum drying to form a thin film. After that, 2 mL of a 4-(2-hydroxyetthyl)-1-piperazineethanesulfonic acid (HEPES, Dojindo Molecular Technologies Inc.) buffer solution was added to the thin film in the vial and the vial was shaken to form multilamellar vesicle solution. To make unilamellar vesicles form, we used mini-extruder which contains a polycarbonate membrane with 100 nm pores. Finally, we prepared the vesicle samples intercalated with DSSN+ and Nile red through the above procedures. Furthermore, we carried out zeta potential measurements (ELS-8000, Otsuka Electronics Co. Ltd.) for characterization of surface charge, and cryogenic transmission electron microscopy (cryo-TEM; Tecnai F20, FEI Com.) technique was employed to observe vesicle's morphologies.

UV-Vis absorption (Lambda 25, Perkin-Elmer) and Fluorescence (QM-3/2004SE, PTI) measurements were done.

In the time-correlated single-photon counting (TCSPC, Nanofinder 30, Tokyo Instruments) study, a pulsed diode laser for sample excitation (PDL 800-B, PICOQUANT), which has 40 MHz of the repetition rate, was used and detector was a single-photon counting avalanche photodiode (SPCM-AQD, PerkinElmer) with a gated photon counter (PMS module, Becker & Hickl GmbH).

In the transient absorption (TA) setup, a femtosecond pulse (130 fs, 650 μJ, 1 kHz)

centered at 800 nm was generated by a standard regenerative-amplified Ti:Sapphire laser (Hurricane, Spectra Physics). The pump pulses were generated by a second harmonic generator (TP1A, Spectra Physics), and sapphire plate (WG31050, Thorlabs) made continuum light which is used as the probe pulse. A delay stage (Daedal 404300XRMP, Parker) was used for the optical time delay between the pump pulse and the continuum pulse. The pump pulse was blocked regularly by a synchronized optical chopper (MC1000, Thorlabs). The probe pulse was detected by photodiodes (2031, New focus) after wavelength selection using a monochromator (250 is/sm, grating of 600 grooves blazed at 750 nm, Chromex). Lastly, a lock-in amplifier (SR830, SRS) obtained the temporal profiles of the TA.

2. Preparation for Photocurrent Measurements.

0.3 mM DMPC and 0.0015 mM DSSN+ solutions, dissolved separately in 2 mL of methanol, were used and 5 mol% of DSSN+ to the DMPC concentration in the vesicles was synthesized. Silicon wafers coated with chromium and gold were prepared and piranha solution (3:1 v/v, concentrated H_2SO_4 to 30% H_2O_2) was used for clean. Also, silicon wafers were rinsed by water and ethanol, and dried by an argon steam. These steps were to make a photovoltaic cell. The gold electrodes were first incubated in 0.5 mM of Nile red (Sigma-Aldrich Co.) dissolved in DMSO for 12 hours, then in 0.05 mM of an 11-mercaptoundecanoic acid (MUA, Sigma-Aldrich Co.) solution for 2 hours, and it was rinsed with deionized water. As a result, gold electrode with a self-assembled monolayer (SAM) of MUA tethered with Nile red was prepared and the electrode was incubated into the above vesicle solutions bearing 5 mol% DSSN+ for 12 hours.

In photocurrent measurements, the surface-modified gold electrode and a Pt electrode were used as the working electrode and counter electrode respectively. Electrolyte was a HEPES buffer solution including 0.1 M ascorbic acid. The photocurrent was measured by using a solar simulator (PEC-L01, Peccell Technologies Inc.) and Keithley 2612A (Keithley Instruments Inc.).

3.3 Results and Discussion

In this study, we synthesized DSSN+ embedded in unilamellar DMPC vesicle in the range 0 to 5 mol% relative to DMPC. DMPC has abilities to form vesicle easily and incorporate hydrophobic components in lipid bilayers. In Figure 3A, typical cryo-TEM image of DMPC vesicle assembled with DSSN+ shows the diameter is from 50 to 120 nm and formation of stable vesicles.

As shown in Figure 3B, when DSSN+ is embedded into lipid bilayers, DSSN+ has the perpendicular alignment to the lipid plane because of charge compensation between the zwitterions in DMPC and terminal quaternary ammonium salts of DSSN+ and hydrophobic attraction between the neutral parts of DSSN+ and alkyl chains of DMPC. To verify the embedding efficiency of DSSN+ in the vesicles, we measured zeta potential in 0.15 M NaCl in pH 7.4 HEPES buffer solution and pure, deionized water. In Figure 3C, as DSSN+ concentration increases up to 3 mol% relative to DMPC, zeta potential value linearly increases, and for over 3 mol%, slight plateau is showed. These results indicate that DSSN+ is more embedded in the vesicle up to 3 mol%, but the embedding efficiency increases slightly in the range of 3 to 5 mol% due to electrostatic repulsion among DSSN+ molecules. To confirm whether or not these results were caused by salt effects in HEPES buffer solution added NaCl, zeta potential measurements were also carried out in pure, deionized water. Zeta potential value also gradually increases over 30 mV with increasing DSSN+ concentration (Figure 3D). The tendency is similar in both buffer solution and deionized water. Therefore, we can confirm that DSSN+ is intercalated in the vesicle up to 5 mol% relative to the DMPC.

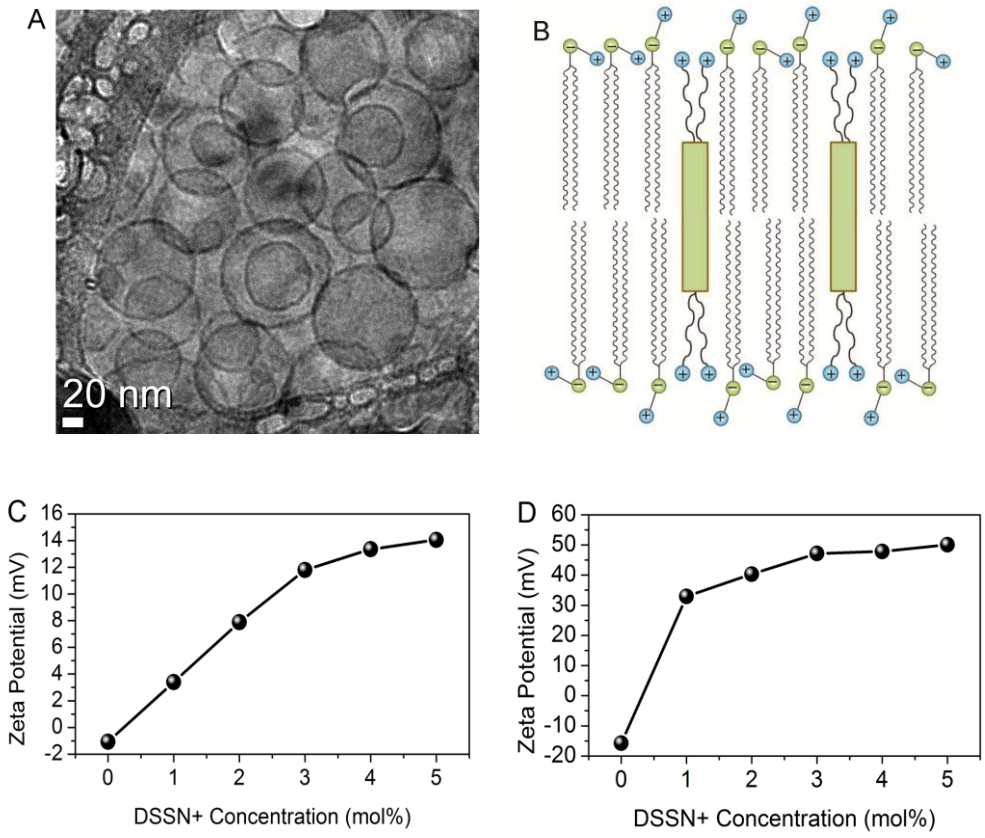

Figure 3. (A) Cryogenic transmission electron microscopy image of DMPC vesicles bearing 2 mol% of DSSN+. (B) Scheme of phospholipid-assembled DSSN+. (C) Zeta potential results of DMPC vesicle solutions in HEPES buffer solution as increasing DSSN+ concentrations in the range 0 to 5 mol% relative to DMPC and (D) in pure, deionized water.

Nile red is one of popular hydrophobic chromophores, which of photophysical properties have been studied. [38-40] In this study, we chose this molecule as an acceptor. As shown in Figure 4, emission spectrum of DSSN+ significantly overlaps with absorption spectrum of Nile red in lipid vesicles. For this reason, FRET between DSSN+ and Nile red in the vesicle can occur effectively.

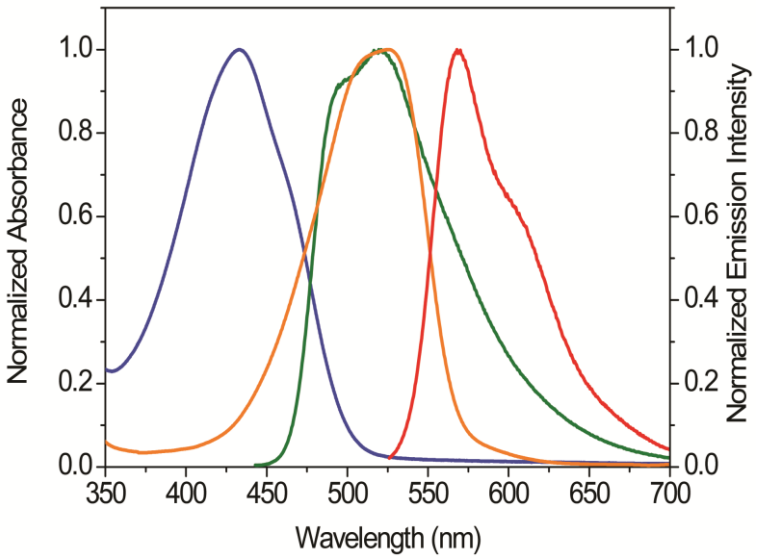

Figure 4. UV absorption and photoluminescence spectra of DSSN+ in lipid vesicles (absorbance = blue, emission = green) and Nile red in toluene (absorbance = orange, emission = red).

The DSSN+ concentration was fixed at 2 mol% whereas the Nile red concentrations varied from 0 to 2.5 mol% relative to DMPC. Both DSSN+ and Nile red are embedded in lipid bilayer. Figure 5A shows the normalized UV absorption spectra of unilamellar DMPC vesicle solutions with increasing Nile red concentrations at a fixed DSSN+ concentration. Nile red absorption constantly increased with increasing concentration. For these same samples, to observe FRET between DSSN+ and Nile red, we applied the steady-state photoluminescence (PL) spectra. Ensemble FRET measurements were done at 400 nm, where the donor solely absorbed photon energy and the acceptor absorbed at minimum, avoiding direct excitation of the Nile red. As a result, emission intensity of Nile red at 620 nm linearly increased as increasing acceptor concentration while emission intensity of DSSN+ decreased. This result means FRET occurred between the donor and acceptor (Figure 5B and 5C).

The time-correlated single photon counting (TCSPC) result shows the lifetime information of FRET from DSSN+ to Nile red embedded in vesicles. We used 405 nm excitation wavelengths to excite the donor only and observed the energy transfer dynamics by monitoring the donor emission and acceptor emission respectively. As shown in Figure 6, when monitoring the Nile red emission at 630 nm, the rise time of Nile red indicates that energy transfer from DSSN+ to Nile red occurs in 200 ps. In here, the fluorescence lifetime is a direct indicator of the energy transfer from the donor to the acceptor.

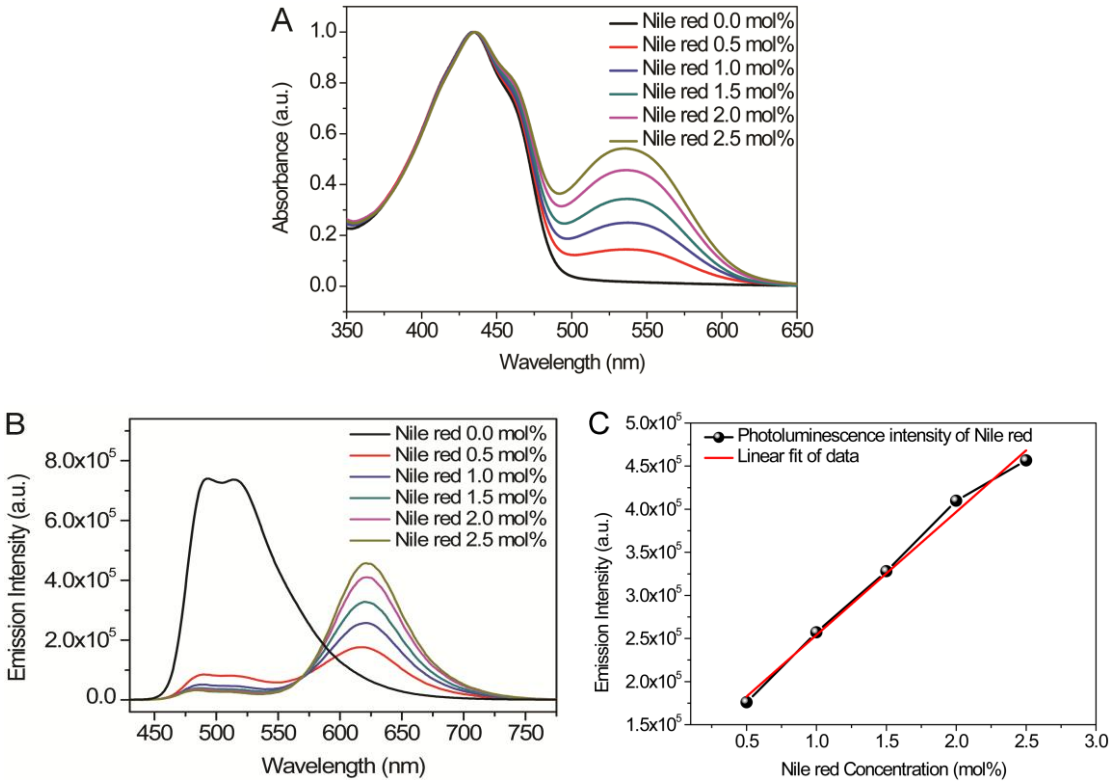

Figure 5. (A) UV absorption spectra of vesicle solutions with increasing Nile red concentrations at a fixed DSSN+ concentration of 2 mol%. (B) PL spectra of vesicle solutions excited at 400 nm, (C) Linear fitting data of the fluorescence maxima at 620 nm with Nile red concentrations.

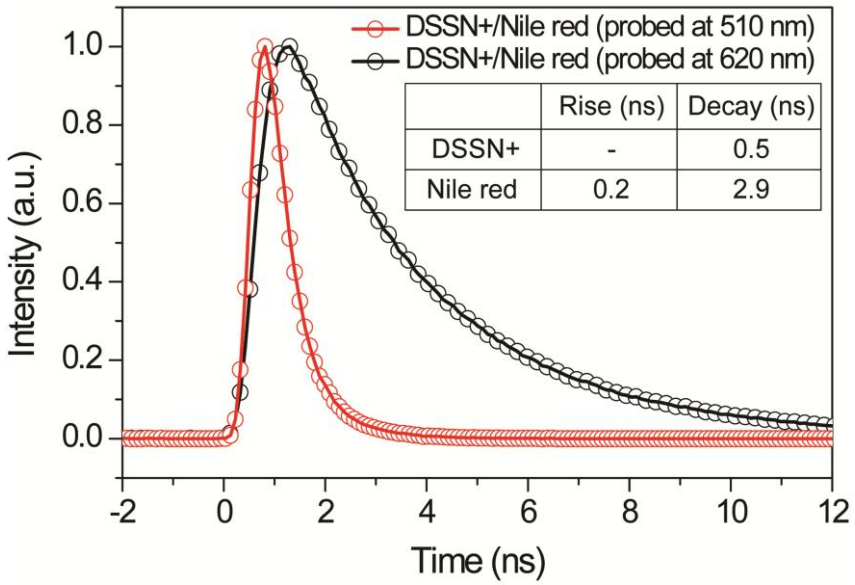

Figure 6. TCSPC results at an emission wavelength of DSSN+ (510 nm) and Nile red (620 nm) respectively.

Figure 7 shows the TA result of DSSN+/Nile red intercalated in vesicles at 400 nm (pump pulse) and 850 nm (probe pulse). We measured the lifetime of DMPC vesicle solutions with increasing Nile red concentrations at fixed DSSN+ concentration of 2 mol%. According to the result, the lifetime has a tendency to decrease as the Nile red concentration increases. The decline in the DSSN+ lifetime explains the energy transfer from the donor to the acceptor effectively.

In addition, we calculated the FRET efficiency (E) from the steady-state PL spectra (Figure 5C) and time-resolved TA spectra (Figure 7) using the following equations.

$$E = \frac{I_A}{I_D + I_A} \quad \text{and} \quad E = 1 - \frac{\tau_{DA}}{\tau_D}$$

For first equation, it is applied when we calculate the FRET efficiency with PL intensity. I_D is the PL intensity of the donor in the presence of an acceptor and I_A is that of the acceptor in the presence of a donor. The FRET efficiency calculated from the PL spectra is shown a rising tendency with increasing Nile red concentration from 68% up to 93%. The FRET efficiency values from PL spectra are shown in Table 1. We confirmed that these values are comparable with the FRET efficiency derived from the lifetime of DSSN+ using second equation. In second equation, τ_{DA} is the lifetime of the donor in the presence of the acceptor and τ_D is that of the donor in the absence of the acceptor. It is reported that the presence of an acceptor results in a decrease in the donor's lifetime.[38] However, when the system is not a homogeneous, the distances between the donor and the acceptor are diverse, and so the donor has multi-exponential decay. For this system, the FRET efficiency is calculated from the average lifetime, $\langle\tau\rangle=\sum_i\alpha_i\tau_i$, where τ_i is the lifetime and α_i is the relative amplitude contribution. Table 1 represents FRET efficiency

values evaluated from two types of equations. Moreover, we tried to estimate the distances between DSSN+ and Nile red. The distances are in range of 32 to 48 Å. These values are enough distances to occur the FRET between DSSN+ and Nile red. These results indicate energy transfer occurs from DSSN+ to Nile red with high FRET efficiency, when the intercalation ratio of Nile red to DSSN+ is increasing. Furthermore, we can expect that our energy transfer system is effective.

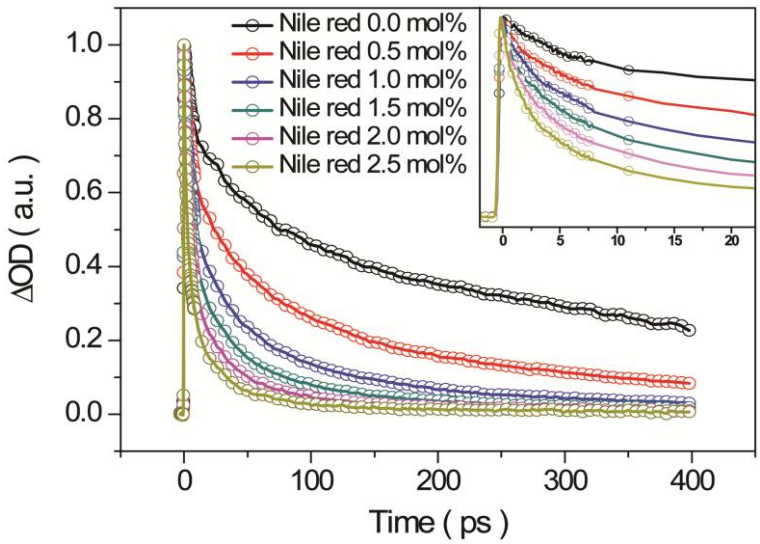

Figure 7. TA results of DMPC vesicle solutions with increasing Nile red concentrations at fixed DSSN+ concentration.

Nile Red (mol%)	FRET Efficiency (E) (Steady-state spectra)	α_1	τ_1 (ps)	α_2	τ_2 (ps)	$\langle\tau\rangle$ (ps)	FRET Efficiency (E) (Time-resolved spectra)
0.0	-		11.5		383.4	152.9	-
0.5	0.68	0.463	9.2	0.229	171.9	62.9	0.59
1.0	0.84	0.455	6.1	0.212	74.2	27.9	0.82
1.5	0.89	0.458	5.0	0.188	56.5	20.0	0.87
2.0	0.92	0.482	3.5	0.189	37.5	13.1	0.91
2.5	0.93	0.509	2.4	0.186	25.1	8.6	0.94

Table 1. FRET efficiency evaluated from steady-state PL spectra and TA spectra, and lifetime components.

To implement the photovoltaic system effectively, the light-harvesting system should be maintained securely on the electrode surfaces. In this study, fabricating the good photovoltaic system was possible because of electrostatic attractions between vesicle surfaces and electrode surfaces. Due to the ionization of carboxylic acid of MUA in HEPES buffer, the MUA-coated gold surface has negative charges. On the other hand, the surface of DMPC vesicle assembled with DSSN+ has positive charges. Therefore, there are electrostatic attractions between vesicle surfaces and electrode MUA-coated electrode surfaces. These interactions make combination of DMPC-assembled DSSN+ layer and MUA-coated electrode more tighten. Moreover, charged species can be deposed on the surface with high ionic strengths because of increasing hydrophobic interactions.[41-44] Therefore deposition efficiency of the lipid bilayer on the MUA-coated surface would be good.

In this study, we prepared a vertical arrangement system of DSSN+ and Nile red on top of the gold electrode. As reported in the experimental section, Nile red was first linked to the gold surface. There are strong binding between lone-pair electrons of nitrogen in the Nile red and the gold surface, and so Nile red can be adsorbed on the gold surface.[45] After that, the electrode was immersed in MUA solution and it is assembled with the lipid layer bearing DSSN+. The electrode structure is shown in Scheme 2.

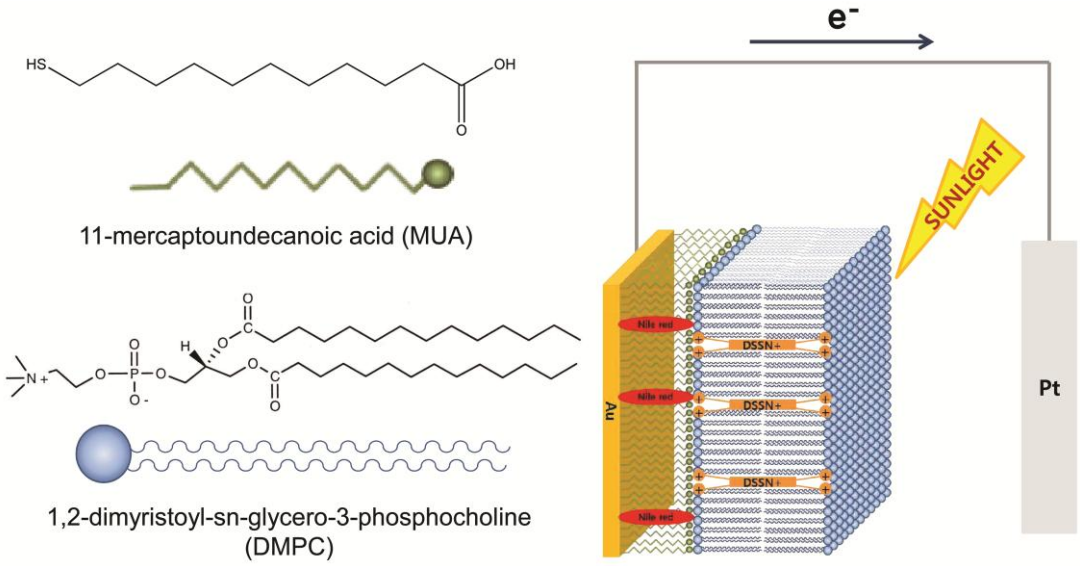

Scheme 2. The structure of the photovoltaic system which has a vertical arrangement of DSSN+ and Nile red on the gold electrode.

To examine the surface morphology of gold electrodes before and after modification, we used atomic force microscopy (AFM). In Figure 8A, the gold electrode only has 1.38 nm of root-mean-square (RMS) roughness. In the case of gold electrodes covered with a monolayer of MUA in which Nile red molecules are tethered, the value of roughness is 1.06 nm. As shown in Figure 8B, the surface looks smooth and it means that MUA is coated on the electrode surface and lots of Nile red molecules are well dispersed in the monolayer of MUA. Figure 8C shows the AFM image of the gold electrode on which MUA bearing Nile red and the lipid bilayer embedded with DSSN+ are vertically assembled, as illustrated in scheme 2. The RMS roughness is 2.09 nm. This case is relatively rough compared to two other cases, but it is enough smooth. One reason of this result is that we carried out AFM microscopy measurement in HEPES buffer medium for the last case, while two other cases were done in the dry state. If we measure in the dry state for the last case, the assembly structure could be destroyed. For this reason, we carried out under this condition.

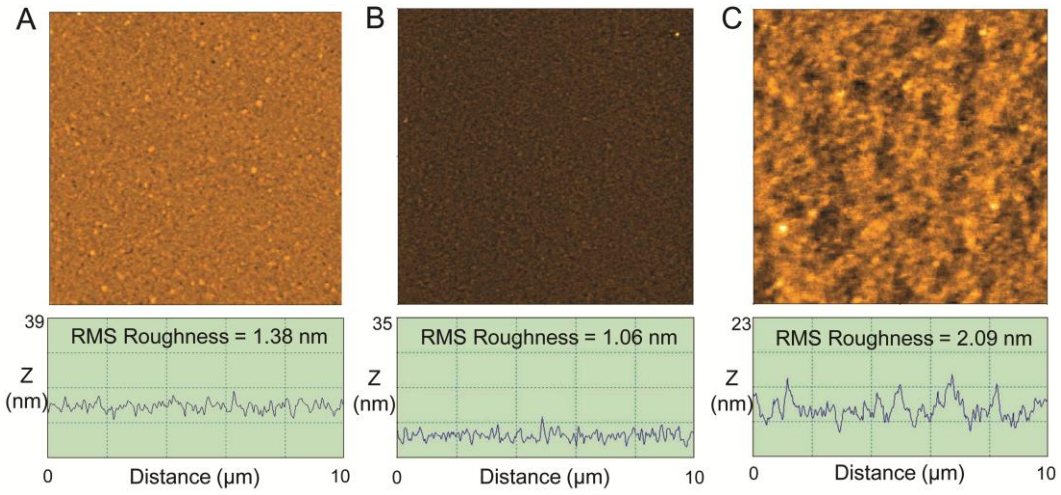

Figure 8. Atomic force microscopy (AFM) images of (A) gold electrodes only and (B) gold electrodes coated with monolayer of MUA in which Nile red molecules are tethered. (C) gold electrodes on which the MUA bearing Nile red and the lipid bilayer modified with DSSN+ are vertically aligned, as shown in Scheme 2.

We measured the photocurrent for three different photovoltaic systems to confirm the enhanced photocurrent generation by FRET between the donor and acceptor. Figure 9 shows structures of three different photovoltaic systems. As shown in Figure 9, structure A is the system with DSSN+ only in vesicles. The gold electrode was coated only with MUA without Nile red, followed by assembling a lipid bilayer bearing DSSN+. In structure B, MUA layer with Nile red is assembled on the gold electrode directly and a lipid bilayer without DSSN+ is placed on the MUA layer. The last system represents the vertical alignment of donor-acceptor (Figure 9C). Nile red tethered in the MUA and DSSN+ incorporated in the DMPC bilayer are vertically aligned on the gold electrode.

Photocurrents were measured under irradiation of white light and results were summarized in Figure 10. When white light irradiated to system A (DSSN+ only), the photocurrent density shows 305 nA/cm^2. Also, in the case of system B (Nile red only), 298 nA/cm^2 of photocurrent is generated. From this result, we might be expected 601 nA/cm^2 of photocurrent density by simple summation. However, the photocurrent is even more enhanced up to 815 nA/cm^2, when the alignment of DSSN+ and Nile red is vertical.

We can specify the energy transfer process according to the alignment of the donor and acceptor. In the first photocurrent generating system (Figure 9A), photoexcited electrons in DSSN+ should be tunneled through the thin insulating layer of the MUA SAM. By the way, the bottom of MUA layer presence adds extra distance between the DSSN+ at the top layer and the electrode, which discourages efficient electron tunneling. As a result, the relatively low photocurrent can be generated. On the other hand, when Nile red is incorporated in the MUA, phtoexcited electrons in DSSN+ can be readily transferred to Nile red because of FRET and they flow to the gold electrode. We can

prove that FRET process between DSSN+ and Nile red in the vertical assembly on the electrode affect the enhanced photocurrent generation. Therefore, the vertical assembly system could be effective to enhance photocurrent generation.

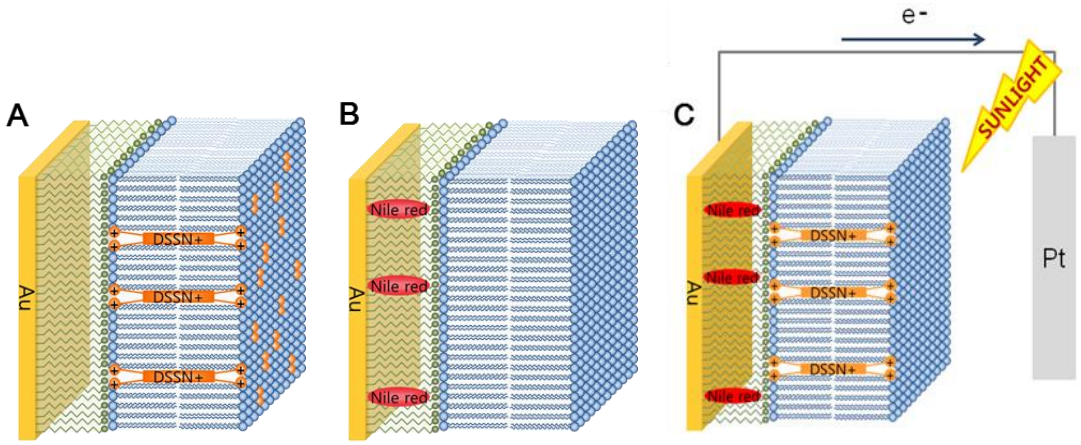

Figure 9. (A) A schematic illustration of the system with only DSSN+ (B) A schematic illustration of the system with only Nile red (C) A schematic illustration of the system where DSSN+ and Nile red are vertically aligned on the gold electrode.

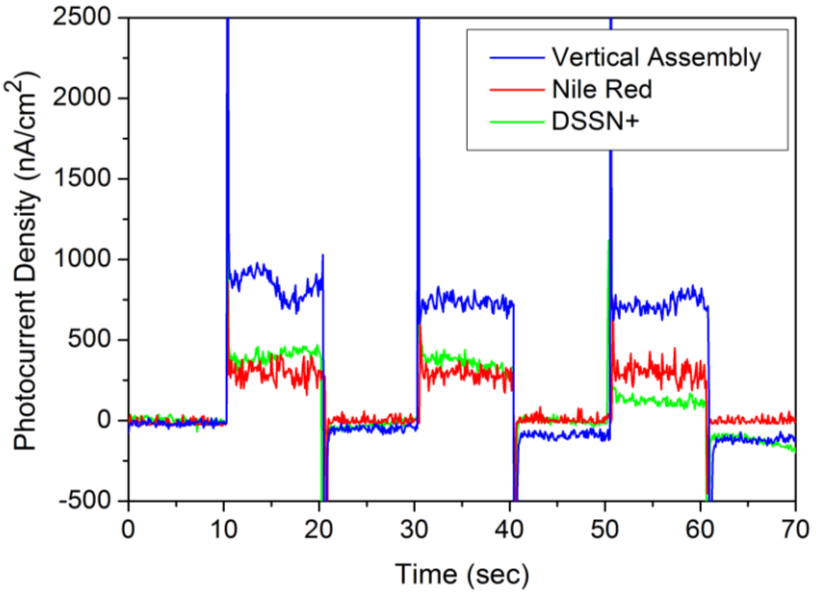

Figure 10. Anodic photocurrents generated from systems with only DSSN+ (green curve) or Nile red (red curve) assembled on MUA-coated gold electrodes, and from the system where Nile red tethered in the SAM and DSSN+ incorporated in the DMPC bilayer are vertically organized on the gold electrode (blue curve).

3.4 Conclusion

In conclusion, we verified that FRET could be occurred between conjugated oligoelectrolytes, DSSN+ and Nile red in DMPC vesicle system. The range of absorption wavelength in Nile red overlaps with the range of emission wavelength in DSSN+. This fact can lead to FRET phenomenon from the donor to the acceptor. To observe FRET, we used steady-state PL spectra and time-resolved spectra, especially TCSPC and TA. We measured the lifetime of DSSN+ with increasing concentration of Nile red. Furthermore, we checked FRET efficiency from PL and TA results, respectively. FRET efficiency values derived from PL and TA results are comparable and it indicates our system is effective. Finally, when we irradiated the white light to three different photovoltaic systems, the photocurrent was generated. The photocurrent value in vertical assembly system on gold electrode which is consist of both DSSN+ and Nile red is higher than that in DSSN+ only or Nile red only assembly system, because of FRET. This study suggests a possibility of implementation of water-based artificial photovoltaic system using phospholipid-assembled conjugated oligoelectrolytes and a dye.

4. References

(1) Maciejewski, A.; Naskrecki, R.; Lorenc, M.; Ziolek, M.; Karolczak, J.; Kubicki, J.; Matysiak, M.; Szymanski, M. *Journal of Molecular Structure* **2000**, *555*, 1-13

(2) Berera, R.; van Grondelle, R.; Kennis, J. T. M. *Photosynth Res* **2009**, *101*, 105-118

(3) Lakowicz, J. R. *Principles of fouroescence Spectroscopy*; Kluwer Academic/Plenum Publishers: New York, 1999.

(4) Das *et al*. *Nano Lett.* **2004**, *4*, 1079-1083.

(5) Ciesielski, P. N.; Scott, A. M.; Faulkner, C. J.; Berron, B. J.; Cliffel, D. E.; Jennings, G. K. *ACS Nano* **2008**, *12*, 2465-2472.

(6) Ciobanu, M.; Kincaid, H. A.; Lo, V.; Dukes, A. D.; Jennings, G. K.; Cliffel, D. E. *J. Electroanal. Chem.* **2007**, *599*, 72-78.

(7) Faulkner, C. J.; Lees, S.; Ciesielski, P. N.; Cliffel, D. E.; Jennings, G. K. *Langmuir* **2008**, *24*, 8409-8412.

(8) Krassen, H.; Schwarze, A.; Friedrich, B.; Ataka, K.; Lenz, O.; Heberle, J. *ACS Nano* **2009**, *3*, 4055-4061.

(9) Terasaki *et al*. *Angew. Chem., Int. Ed.* **2009**, *48*, 1585-1587.

(10) Terasaki *et al*. *Biochim. Biophys. Acta, Bioenerg.* **2007**, *1767*, 653-659.

(11) Yehezkeh, O.; Wilner, O. I.; Tel-Vered, R.; Roizman-Sade, D.; Nechushtai, R.; Willner, I. *J. Phys. Chem. B* **2010**, *114*, 14383-14388.

(12) Maly, J.; Krejci, J.; Ilie, M.; Jakubka, L.; Masojidek, J.; Pilloton, R.; Sameh, K.; Steffan, P.; Stryhal, Z.; Sugiura, M. *Anal. Bioanal. Chem.* **2005**, *381*, 1558-1567.

(13) Badura, A.; Esper, B.; Ataka, K.; Grunwald, C.; Woll, C.; Kuhlmann, J.; Heberle, J.; Rogner, M. *Photochem. Photobiol.* **2006**, *82*, 1385-1390.

(14) Maly, J.; Masojidek, J.; Masci, A.; Ilie, M.; Cianci, E.; Foglietti, V.; Vastarella, W.; Pilloton, R. *Biosens. Bioelectron.* **2005**, *21*, 923-932.

(15) Touloupakis, E.; Boutopoulos, C.; Buonasera, K.; Zergioti, I.; Giardi, M. T. *Anal. Bioanal. Chem.* **2012**, *402*, 3237-3244.

(16) Bhalla, V.; Zazubovich, V. *Anal. Chim. Acta* **2011**, *707*, 184-190.

(17) Kasuno, M.; Torimura, M.; Tsukatani, Y.; Murakami, D.; Hanada, S.; Matsushita, T.; Tao, H. *J. Electroanal. Chem.* **2009**, *636*, 101-106.

(18) Amao, Y.; Kuroki, A. *Electrochemistry* **2009**, *77*, 862-864.

(19) Terasaki, N.; Iwai, M.; Yamamoto, N.; Hiraga, T.; Yamada, S.; Inoue, Y. *Thin Solid Films* **2008**, 516, 2553-2557.

(20) Jin, Y.; Honig, T.; Ron, I.; Friedman N.; Sheves M.; Cahen D. *Chem. Soc. Rev.* **2008**, *37*, 2422-2432.

(21) Boucher F.; Taneva S. G.; Elouatik S.; Déry M.; Messaoudi S.; Harvey-Girard E.; Beaudoin N. *Biophys. J.* **1996**, *70*, 948-961.

(22) Chu, L. K.; Yen, C. W.; El-Sayed, M. A. *J. Phys. Chem. C* **2010**, *114*, 15358-15363.

(23) Yen, C. W.; Hayden, S. C.; Dreaden, E. C.; Szymanski, P.; El-Sayed, M. A. *Nano Lett.* **2011**, *11*, 3821-3826.

(24) Lee, J. W.; Collins, R. T.; Greenbaum, E. *J. Phys. Chem. B* **1998**, *102*, 2095-2100.

(25) Balzani, V.; Credi, A.; Venturi, M. *ChemSusChem* 2008, 1, 26-58.

(26) Hollander M. J.; Magis, J. G.; Fuchsenberger, P.; Aartsma, T. J.; Jones, M. R.; Frese, R. N. *Langmuir* **2011**, *27*, 10282-10294.

(27) Taffa, D. H.; Kathiresan, M.; Arnold, T.; Walder, L.; Erbacher, M.; Bauer, D.; Montforts, F. P.; Nordmann, J.; Haase, M. *J. Photochem. Photobiol., A* **2010**, *216*, 35-43.

(28) Govorov, A. O.; Carmeli, I. *Nano Lett.* **2007**, *7*, 620-625.

(29) Frolov, L.; Rosenwaks, Y.; Richter, S.; Carmeli, C.; Carmeli, I. *J. Phys. Chem. C* **2008**, *112*, 13426-13430.

(30) Giardi, M. T.; Scognamiglio, V.; Rea, G.; Rodio, G.; Antonacci, A.; Lambreva, M.; Pezzotti, G.; Johanningmeier, U. *Biosens. Bioelectron.* **2009**, *25*, 294-300.

(31) Koo, H. J.; Chang, S. T.; Slocik, J. M.; Naik, R. R.; Velev, O. D. *J. Mater. Chem.* **2011**, *21*, 72-79.

(32) Jiang, K.; Xie, H.; Zhan, W. *Langmuir* **2009**, *25*, 11129-11136.

(33) Zhan, W.; Jiang, K.; Smith, M. D.; Bostic, H. E.; Best, M. D.; Auad, M. L.; Ruppel, J. V.; Kim, C.; Zhang, X. P. *Langmuir* **2010**, *26*, 15671-15679.

(34) Zhan, W.; Jiang, K. *Langmuir* **2008**, *24*, 13258-13261.

(35) Ochiai, T.; Nagata, M.; Shimoyama, K.; Amano, M.; Kondo, M.; Dewa, T.; Hashimoto, H.; Nango, M. *Langmuir* **2010**, *26*, 14419-14422.

(36) Ortony, J. H.; Chatterjee, T.; Garner, L. E; Chworos, A.; Mikhailovsky, A.; Kramer, E. J.; Bazan, G. C. *J. Am. Chem. Soc.* **2011**, *133*, 8380-8387.

(37) Garner, L. E.; Park, J.; Dyar, S. M.; Chworos, A.; Sumner, J. J.; Bazan, G. C. *J. Am. Chem. Soc.* **2010**, *132*, 10042-10052.

(38) Lakowicz, J. R. *Principles of Fluorescence Spectroscopy*; Kluwer Academic/Plenum Publishers: New York, 1999.

(39) Krishna, M. M. G. *J. Phys. Chem. A* **1999**, *103*, 3589-3595.

(40) Jain, B.; Das, K. *Chem. Phys. Lett.* **2006**, *433*, 170-174.

(41) Dobrynin, A. V.; Deshkovski, A.; Rubinstein, M. *Macromolecules* **2001**, *34*, 3421-3436.

(42) Dobrynin, A. V.; Rubinstein, M. *Macromolecules* **2002**, *35*, 2754-2768.

(43) Dobrynin, A. V.; Rubinstein, M. *J. Phys. Chem. B* **2003**, *107*, 8260-8269.

(44) Park, J.; Hammond, P. T. *Macromolecules* **2005**, *38*, 10542-10550.

(45) Tseng, W. L.; Lee, K. H.; Chang, H. T. *Langmuir* **2005**, *21*, 10676-10683.

Appendix

1. Bio-imaging using Fluorescent Compound produced from Resveratrol and Resveratrol derivative.

1.1 Introduction

Fluorescence is very crucial in the detection and study of biological phenomena and fluorescence microscopy. Fluorescence microscopy has contributed to the study of biological and cellular events. Fluorophores have played an important role for imaging.[1] Fluorescent imaging techniques have developed rapidly from confocal microscopy to super resolution microscopy such as STORM, PLAM and STED in the several decades.[2-5] Development of fluorescence microscopy techniques has been related to fluorophores which include quantum dots (QD) and synthetic or natural organic/inorganic compounds.[6] Although these fluorophores are used in fluorescent imaging extensively, their cytotoxicity problem has been often discussed. In biological imaging study, cytotoxicity can lead to cell damage and unfavorable events. In the case of QD, the nanotoxicity induced from the size and leakage of inner materials by oxidation or chemical reaction may contribute to cytotoxicity.[7-9] Organic fluorophores also have low or high toxicity.

We reported a new, highly fluorescent compound produced from resveratrol by UV irradiation in recent study. Besides, we discovered a new fluorescent photoproduct of resveratrol glucoside generated by a similar photoreaction of resveratrol. These new two compounds has no cytotoxicity and their photophysical properties are similar. In this study, we suggested that they can be used in imaging studies of various bio-targets.

1.2 Experimental

1. Synthesis of Resveratrone and Resveratrone glucoside.

Resveratrone is produced by photochemical reaction of resveratrol. We irradiated UV light to 125 μM resveratrol in methanol. To isolate pure resveratrone from other side products, we used preparatory thin layer chromatography. Here, the mixture eluent of methanol and methylene chloride (1:20) is used as the mobile phase.

Resveratrone glucoside is also generated by photochemical reaction of resvertrol glucoside (or polydatin) in a similar way of resveratrone. UV light is irradiated to 125 μM resveratrol glucoside in methanol for 4 times longer time, compared to resveratrone. Pure resveratrone glucoside is isolated by high performance liquid chromatography where the mobile phase was mixture solution of 30% methanol + 10% acetonitrile + 60% water with flow 5 ml min^{-1}.

2. Sample Preparation.

1) *Escherichia coli.* of BL21(De3) type

Resveratorne glucoside powder was dissolved in Lysogeny broth medium (LB) and *E. coli* was incubated in this 1 mM LB solution dissolved resveratrone glucoside during overnight. After centrifugation at 4,000 rpm for 3 min, the supernatant is removed and PBS buffer was added for washing. These processes were repeated three times and then *E. coli* was placed on the coverglass-bottom dish. We also prepared *E. coli* sample without resveratrone glucoside to compare the fluorescence intensity.

2) Yeast

We used *S. Cerevisiae* (Sigma, YSC1). They were cultured in 10 mg/mL YPD broth (Sigma, Y1375) with or without 300 μM resveratrone or resveratrone glucoside for 24 hours. Imaging medium was prepared by dissolving yeast nitrogen base with amino acids and β-D-glucose because of strong autofluorescence of YPD broth. After centrifugation at 4,000 rpm for 1 min, the supernatant was removed and yeast was resuspended in the medium. The washing step was repeated 3 times and then yeast was placed on the coverglass-bottom dish.

3) HeLa cells

HeLa cells were cultured in DMEM media with 10% FBS and then removed the media. Methanol fixation was applied to increase the cell membrane permeability and then washed with PBS buffer. After that, HeLa cells were incubated in 300 μM PBS dissolved resveratrone or resveratrone glucoside for 6 hours. Mowiol was used as the mounting medium.

1.3 Results and Discussion

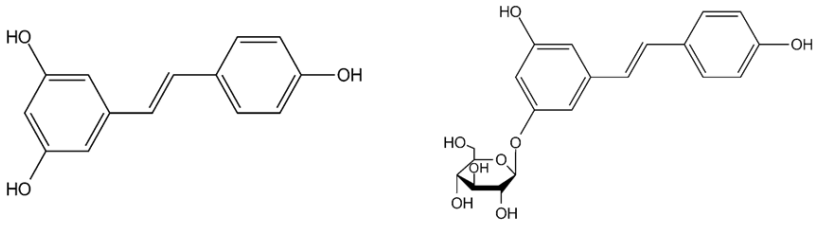

Figure 1. Structures of resveratrol, 1, and resveratrol glucoside, 2.

Resveratrol, 1, is a compound found in berries, grapes, red wine, grape juice and nuts. Many researchers confirmed potential medical functions of resveratrol such as anti-cancer, anti-oxidant and lifespan extension. For this reason, resveratrol has been intensively studied in a wide range of field. In previous study, we discovered a new fluorescent compound named "resveratrone" that results from UV irradiation of non-fluorescent molecule, trans-resveratrol.[10] We identified a structure of resveratrone using ^{1}H-NMR and ^{13}C-NMR analysis. This molecule is produced by simple method and it has various physical properties which can be applied to fluorescence imaging applications. Resveratrone has a high fluorescent quantum yield and a large Stokes' shift which makes it possible to multicolor fluorescent labeling and live bio imaging. Moreover, it shows one-photon and two-photon emission characteristics.

Resveratrol glucoside, 2, is a natural resveratrol derivative which is more contained in grapes and Itadori tea than resveratrol. We also confirmed the generation of

resveratrone glucoside which is a highly fluorescent compound produced by UV irradiation from non-fluorescent resveratrol glucoside. The photoreaction occurred in the similar reaction of resveratrol and the physical properties of resveratrone glucoside are comparable to those of resveratrone. It has also one-photon and two-photon emission characteristics and large Stokes' shift like resveratrone. In addition, it has a higher water solubility than resveratrone. From these properties, we can expect that resveratrone glucoside has a potential to be used in biological study.

Fig. 2a and 2b are the chemical structures of resveratrone and resveratrone glucoside. Resveratrone glucoside is produced in a similar way to resveratrone and we should irradiate UV light for about 4 times longer time than resveratrone. Pure resveratrone is obtained by preparatory thin layer chromatography,[10] while resveratrone glucoside is purified by preparatory HPLC because of the low polarity difference among side products. Figure 2c and 2d show the excitation and emission spectra of in water. Emission is shown when excited at 390 nm. Also, two cuvette images represent two-photon emission properties of two fluorescent photoproducts. Moreover, to check the existence of the glucoside group, we employed ^{1}H-NMR analysis. Figure 3 shows the result of ^{1}H-NMR measurement.

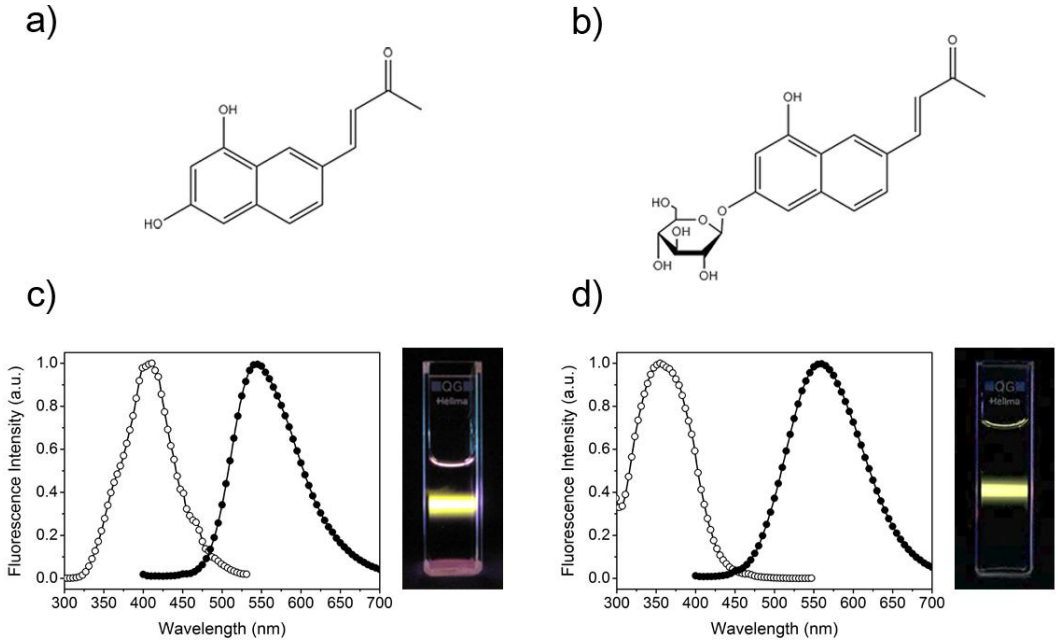

Figure 2. a) The chemical structure of resveratrone. b) The chemical structure of resveratrone-glucoside. c) Excitation (open circles) and emission (solid circles) spectra of resveratrone (Left). Two-photon image in quartz cuvette when photoexcited at 800 nm (Right). d) Excitation (open circles) and emission (solid circles) spectra of resveratrone glucoside (Left). Photograph of two-photon image in quartz cuvette when photoexcited at 800 nm (Right).

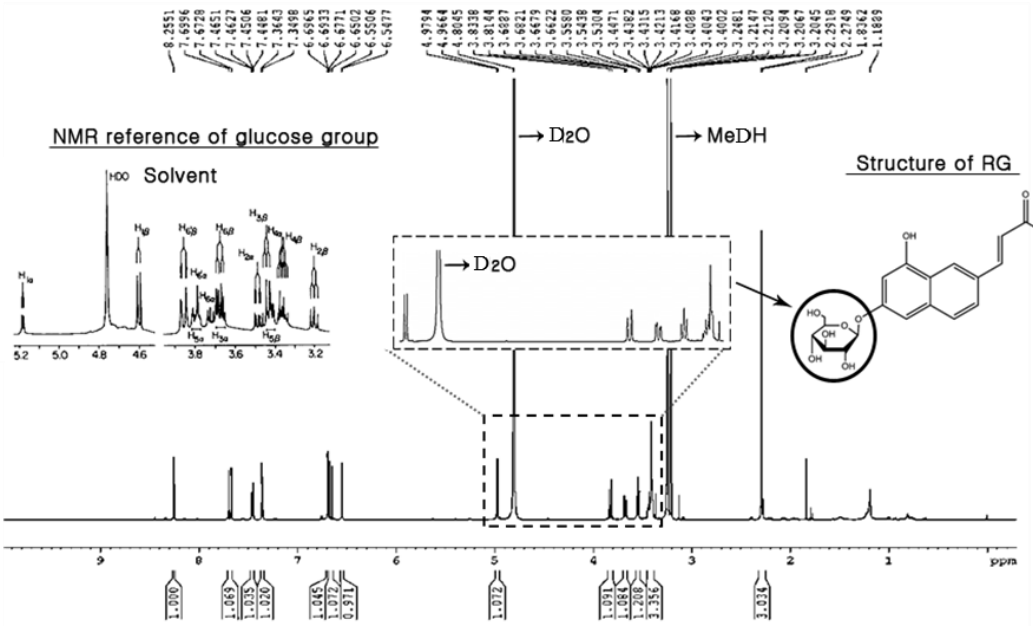

Figure 3. [1]H-NMR spectrum of resveratrone glucoside at 600MHz. The magnified image is representative of β-D-glucose.

Furthermore, to identify whether resveratrone and resveratrone glucoside are not cytotoxic, we tested trypan blue exclusion assay and western blot analysis. As result of these experiments, we confirmed that resveratrone and resveratrone glucoside are not cytotoxic and safe compounds. We applied resveratrone and resveratrone glucoside to various biological specimens to support the possibilities as fluorophores for fluorescent imaging. We obtained confocal images and used a 458 nm light source for one-photon and 800 nm light source for two-photon. First, we treated 1 mM resveratrone glucoside to *Escherichia coli*. BL21(De3). As shown in Figure 4, autofluorescence of unstained *E. coli* is weak (first row), however, the fluorescence of *E. coli* stained with resveratrone glucoside is strong in the case of both one and two-photon excitation. (second row). Figure 5 shows confocal images of yeast. Images of yeast treated with resveratrone or resveratrone glucoside showed a distinctive fluorescence, compared to control images of untreated yeast. In this time, the concentration of resveratrone or resveratrone glucoside solution is 300 μM. We also treated two fluorescent compound to the HeLa cell which has bigger size than *E. coli* and yeast. We injected 300 μM resveratrone or resveratrone glucoside to HeLa cell fixed with methanol. Here, methanol fixation increased the cell membrane permeability,[11] so that it is possible to stain the whole body of cell. In Figure 6, confocal images of HeLa cell stained both resveratrone and resveratrone glucoside show strong emission (second and third rows), while the control images of HeLa cell only is not seen autofluorescence (first row). In addition, to ensure whether fluorescence compounds get into internal of the cell or not, we tried to measure z-sectioning scan. Figure 7 shows z-sectioning images of HeLa cell treated with resveratrone glucoside.

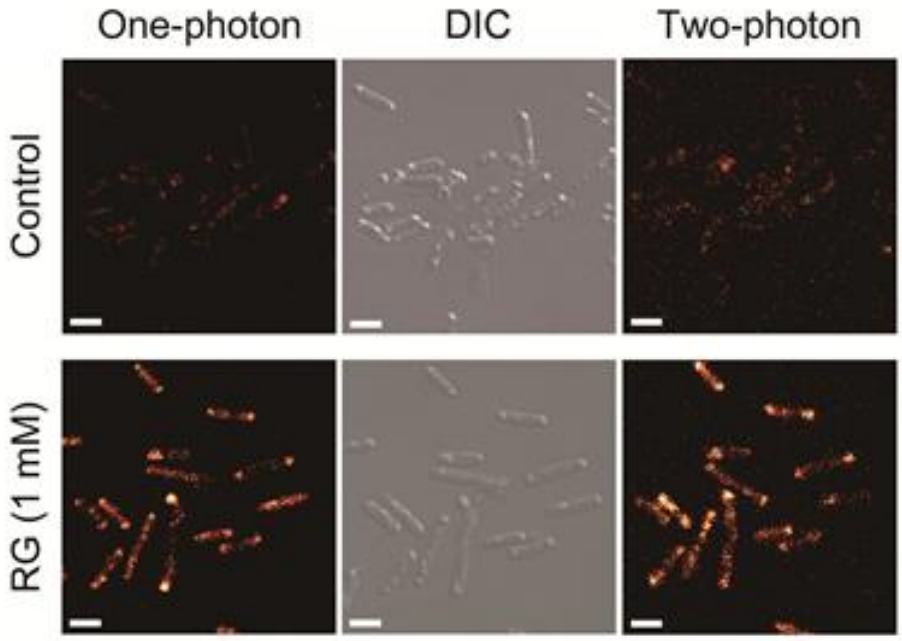

Figure 4. Confocal images of *E.coli* with one-photon (458 nm, left), DIC (middle), and two-photon (800 nm, right) imaging. The first row shows images of the *E.coli* only, and the second row images are 1 mM resveratrone glucoside fluorescence in *E.coli.* The scale bar represents 2.5μm.

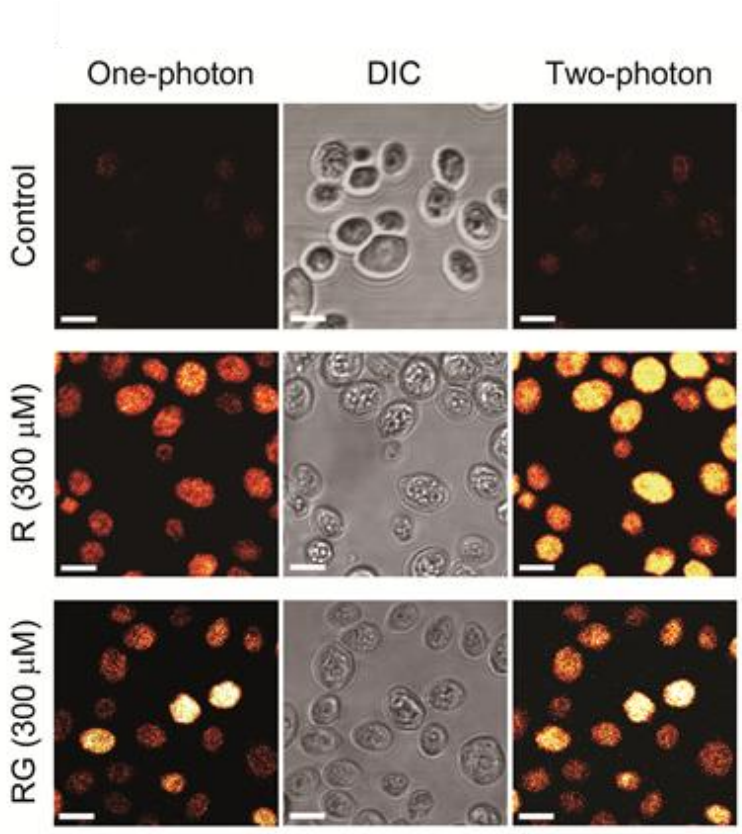

Figure 5. Confocal images of yeast with one-photon (458 nm, left), DIC (middle), and two-photon (800 nm, right) imaging. The first row shows images of the yeast only, and the middle row images are 300 μM resveratrone fluorescence in yeast. The bottom row shows images of yeast stained with 300 μM resveratrone glucoside. The scale bar represents 5μm.

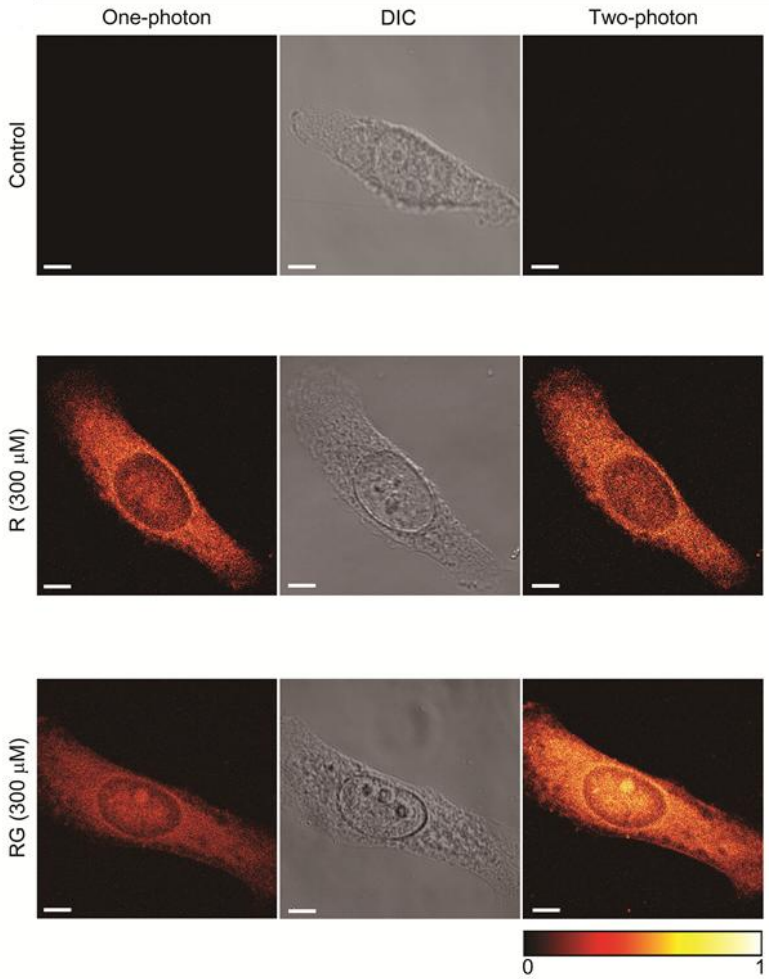

Figure 6. Confocal images of HeLa cell with one-photon (458 nm, left), DIC (middle), and two-photon (800 nm, right) imaging. The first row shows images of the HeLa cell only, and the middle row images are 300 μM resveratrone fluorescence in HeLa cell. The bottom row shows images of HeLa cell stained with 300 μM resveratrone glucoside. The scale bar represents 5μm.

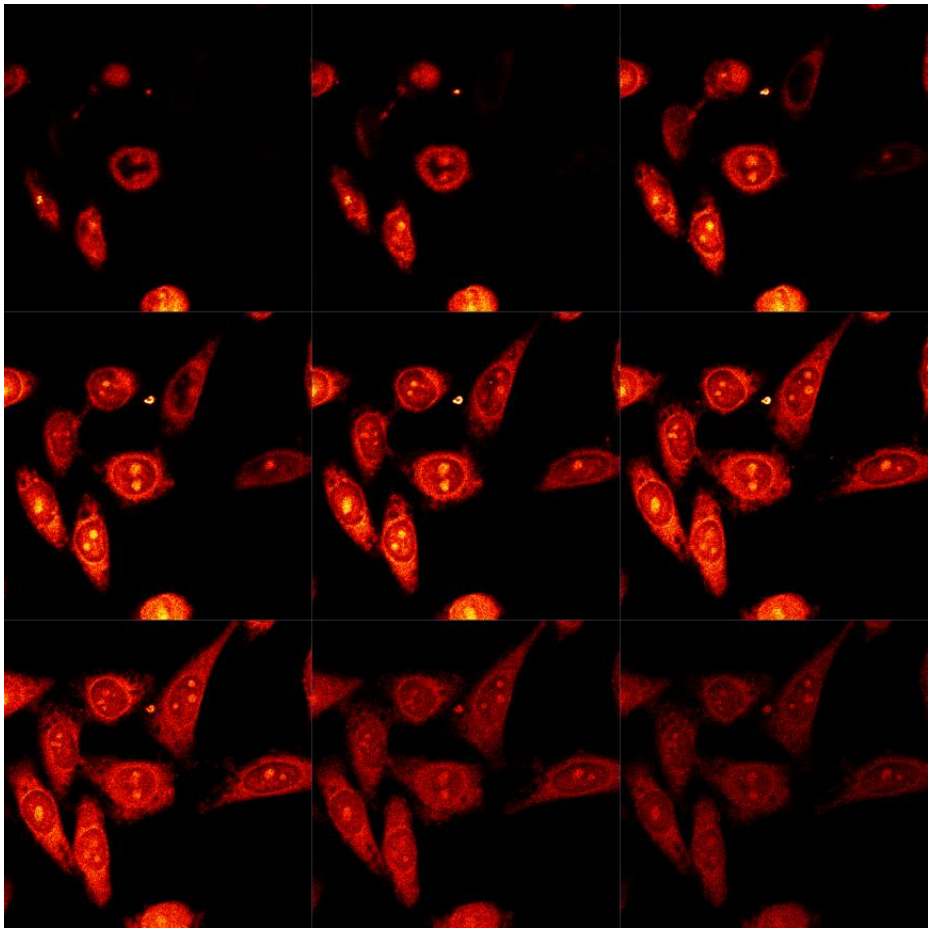

Figure 7. Z-sectioning images of resveratrone glucoside stained HeLa cell with 405 nm excitation.

1.4 Conclusion

To sum up, we identified new fluorescent photoproducts produced by UV irradiation from non-fluorescent compound, which are called resveratrone and resveratrone glucoside respectively. Photophysical properties of resveratrone glucoside are comparable to those of resveratrone. These molecules have high quantum yield, one-photon emission and two-photon emission characteristics. We also showed the possibilities as fluorophores for fluorescent imaging by applying them to various biological specimens such as *E.coli*, yeast and HeLa cell. Furthermore, we expect that resveratrone glucoside has more potential to be used in the wide range of bio application, because resveratrone glucoside has higher water solubility than resveratrone.

1.5 References

(1) V. Ntziachristos, *Annu. Rev. Biomed. Eng.* **2006**, *8*, 1-33.

(2) E. Betzig, G. H. Patterson, R. Sougrat, O. W. Lindwasser, S. Olenych, J. S. Bonifacino, M. W. Davidson, J. Lippincott-Schwartz, H. F. Hess, *Science* **2006**, *313*, 1642-1645.

(3) S. W. Hell, *Science* **2007**, *316*, 1153-1158.

(4) S. W. Hell, J. Wichmann, *Opt. Lett.* **1994**, *19*, 780-782.

(5) M. J. Rust, M. Bates, X. W. Zhuang, *Nat. Methods.* **2006**, *3*, 793-795.

(6) M. Sameiro, T. Goncalves, *Chem. Rev.* **2009**, *109*, 190-212.

(7) U. Resch-Genger, M. Grabolle, S. Cavaliere-Jaricot, R. Nitschke, T. Nann, *Nat. Methods.* **2008**, *5*, 763-775.

(8) N. Lewinski, V. Colvin, R. Drezek, *Small* **2008**, *4*, 26-49.

(9) A. Shiohara, A. Hoshino, K. Hanaki, K. Suzuki, K. Yamamoto, *Microbiol.*

(10) I. Yang, E. Kim, J. Kang, H. Han, S. Sul, S. B. Park, S. K. Kim, *Chem. Commun.* **2012**, *48*, 3839-3841.

(11) Y. Williams, S. Byrne, M. Bashir, A. Davies, A. Whelan, Y. Gun'ko, D. Kelleher, Y.Volkov, *J. Microsc.* **2008**, *232*, 91-98.

국문초록

시분해 분광학 연구는 분자의 동력학 및 광물리적 특성을 규명하는데 필수적이며, 시분해 분광법을 기반으로 하는 연구에 대한 관심은 지속적으로 높아지고 있다. 펨토초 순간 흡수 분광법 및 시간 상관 단일 광자 계수법과 같은 시분해 분광학 기술들은 빛에 의해 유도된 순간 생성물의 전이 상태에서의 전자에 대한 동력학 정보를 제공한다. 이 논문은 이러한 시분해 분광학 기술을 이용하여 물 기반의 인공 태양전지 시스템을 구현하기 위해 사용된 두 분자 간의 에너지 전이를 확인한 내용을 담고 있다.

친환경 시스템 발전에 이바지하는 물 기반의 인공 태양전지에 대한 연구 관심은 나날이 증가하고 있다. 본 연구는 시분해 분광법의 응용 연구로서 자연에서의 photosystem II 단백질의 역할을 모사한 물 기반의 인공 태양전지 시스템을 구현하기 위해 DSSN+와 Nile red라는 두 분자를 DMPC 베지클에 집적하였다. DSSN+와 Nile red는 두 가지의 다른 파장 영역의 빛을 흡수할 수 있으며, DSSN+의 형광 파장 범위와 Nile red의 흡수 파장 범위는 잘 겹치게 된다. 이후 DSSN+에서 Nile red로의 에너지 전이를 정류상태 형광 분광법과 시분해 분광법인 시간 상관 단일 광자 계수법과 순간 흡수 분광법을 통해 설명하였다. 아울러 전이상태 수명시간과 형광 세기 수치를 이용하여 DSSN+와 Nile red 사이의 형광 공명 에너지 전이 효율을 계산해 보았으며, 높은 효율을 가지고 에너지가 전이됨을 확인하였다. 또한 광전류가 생성되는

새로운 시스템의 인공 태양전지 구조를 제안하는 연구를 수행하였다.

주요어: 순간 흡수 분광법, 시간 상관 단일 광자 계수법, 형광 공명 에너지 전이, DSSN+, 광전류

학 번: 2011-20301

감사의 글

2011년 1월, MRD에 처음 들어와 2년이 흐른 지금 MRD에서의 생활은 저에겐 하루하루가 모두 값지고 잊지 못할 추억이 된 것 같습니다. 학부 때 막연히 화학이 너무 좋아서 공부를 더 해보자 라는 생각에 석사과정을 입학했던 탓인지 대학원을 입학하고 몇 개월은 처음 접해 보는 수많은 과학적 정보, 기술들과 용어로 쉽게 의견을 낼 수 없었던, 좌절과 후회의 나날이었습니다. 하지만, 석사과정 기간 동안 많이 배우고 경험할 수 있었기에 이전보다는 많이 성장할 수 있었던 것 같습니다. 무엇보다 무사히 석사과정을 마칠 수 있었던 것은 항상 저를 응원해주시고 따끔하면서도 따뜻한 조언을 해주신 많은 분들의 도움이 있었기 때문이라고 생각합니다. 먼저, 부족한 저에게 용기를 주시며 언제나 관심을 가지고 다양한 경험을 해볼 수 있도록 기회를 주신 김성근 선생님께 진심으로 감사 드립니다. 선생님께서 들려주신 많은 이야기들로부터 연구란 무엇인지에 대해 배울 수 있었으며, 연구의 즐거움을 느낄 수 있었습니다.

논문 심사를 해주신 서정쌍 교수님, 신석민 교수님께 감사의 말씀을 드립니다. 바쁘신 중에도 저의 논문 심사 때문에 시간을 내주시고 많은 관심을 가져주시며 발전할 수 있도록 조언을 주신 교수님들께 감사 드립니다.

석사과정 동안 실험실에 있으면서 함께 지낸 MRD 멤버들에게도 감사하다는 말과, 더 많은 시간을 함께 못한 데에 대한 아쉬움을 전하고 싶습니다. 2년

동안 실험실 생활을 하면서 많은 분들의 도움을 받은 것 같습니다. 특히, 처음 MRD에 들어와 팀을 결정하는데 많은 고민을 하던 제게 먼저 손 내밀어 주신 양일승 박사님께 정말 감사 드립니다. 항상 챙겨주시고 실험뿐만 아니라 여러 가지를 알려주신 박사님 덕분에 많은 것을 배울 수 있었습니다. 그리고 팀장으로 항상 듬직하게 팀원들을 이끄는 선진오빠, 매너 좋고 인기 많은 종우오빠, 똑똑하고 열심히 하는 도익이와 은학이, 동고동락한 팀원으로써 감사하다는 말을 전하고 싶습니다. 따끔한 조언을 해주시며 부지런함과 성실함을 배우게 되는 현이오빠와 남두오빠, 실험실에 있으면서 언제나 저를 챙겨주는 친언니 같은 지희언니 그리고 다른 선/후배 분들께도 여기에 다 적지 못하지만 감사하다는 말을 드리고 싶습니다. MRD에서 보낸 2년 동안의 생활은 앞으로 어떤 일이든 탄탄한 밑거름이 될 수 있는 소중한 경험이라고 생각합니다.

마지막으로 글로는 다 표현하기 부족하지만 언제나 저를 믿고 큰 사랑과 애정으로 든든하게 제 곁을 지켜주는 부모님, 그리고 항상 웃음을 선사하는 듬직한 동생 정석이, 너무나 많이 사랑하고 감사합니다.